Journal of Energy, Heat and Mass Transfer, Vol.16, 35-45 (1994)

Wetting of Dispersed Flow Film Boiling in Heated Bends

F.MAYINGER, M.J.WANG AND G.LAUTENSCHLAGER

Lehrstuhl A für Thermodynamik, Technische Universität München, 80290 Munchen, FR Germany

Abstract

Dispersed flow film boiling has been investigated experimentally under a wide range of boundary conditions in the 90-deg heated circular bends. Wetting phenomenon was confirmed from measurements of the wall temperature distribution and the liquid distribution. This phenomenon, revealed from the mechanistic analysis of droplet dynamics, is attributed to the intensive direct impingement of droplets on the wall. It is further indicated from the parametric study that the onset of wetting depends critically on the temperature gradient in the boundary layer and the droplet deposition flux. The wetting development in circumference is governed by the secondary vapor flow and the gravitational force.

Introduction

Dispersed flow in the present study is referred to the flow pattern in post-dryout film boiling, characterized by liquid droplets in dispersed form entrained in a continuous flowing vapor. Dispersed flow film boiling is of great importance in many industrial applications, for example, in the design and operation of once-through steam generators, in the analysis of a hypothetical loss-of-coolant accident in nuclear reactor systems and in the evaluation of some metallurgical and cryogenic processes. The heat transfer mechanism of dispersed flow in the high wall- superheat region has been well investigated for simple geometries [1-2]. It is generally known that dispersed flow in this region is associated with thermal non-equilibrium and low heat transfer coefficients. Droplet interactions with the wall usually result in a form of dry impact, i.e. most droplets only enter the thermal boundary layer, but do not impinge directly on the wall. Consequently, the vapor convection dominates the wall heat transfer.

However this heat transfer mechanism can be altered with the establishment of a continuous liquid film staying along the hot wall i.e. wetting, when the dispersed flow is encountered to some obstructs or the change of the flow geometry [3]. By the evaporation of the liquid film on the surface, wetting brings about significant augmentation in heat transfer. There are numerous investigations on this aspect reported in literature [3-9]. One of the critical issues of these researches is the condition under which wetting takes place. Fundamental studies on wetting by small mass of liquid droplets indicate that the wetting temperature, named also as the Leidenfrost temperature, is a function of surface condition, reduced system pressure, subcooling and Weber number of the dorplet. Based on various experimental data, some empirical correlations were proposed to calculate the wetting temperature [4-5]. Surface wetting by flowing fluid under film boiling is more complicated and has been revealed to be governed by different controlling mechanisms. Conditions that mark the end of stable film boiling can be attributed either to the instability at vapor-liquid interface during the flooding phase [6-7] or to the dispersed droplet cooling [3]. The former depends on the thermal, hydrodynamic and geometric parameters pertinent to the system, whereas the latter is related more to the dynamics of individual droplets, vapor conditions and heated surface properties. Hence there is no unique wetting temperature. For example, Hein [6] revealed from his flooding experiments that for refrigerant Freon-12, the wetting temperature ranges from 30 to 50 K above the saturation temperature for a reduced pressure less than 0.5 and a few degrees beyond the saturtion point for higher reduced pressures. Typical

empirical correlations like those of Plummer et al. [8] and Groeneveld and Stewart [9] give the wetting temperature only with limited validation.

This paper studies the wetting phenomenon of dispersed flow film boiling in the 90-deg circular heated bend - a common flow geometry in practice. Different from the case in a straight channel, the basic flow field in a bend is strongly influenced by the centrifugal force and the induced secondary flow [10]. In the core of the flow, the fast-moving fluid is centrifugally driven from the inner to the outer side, whereas in the wall region the pressure force is overwhelming, and the slow-moving fluid is forced to flow from the outer to the inner side of the bend. A typical flow structure in the cross-section is illustrated in figure 1.

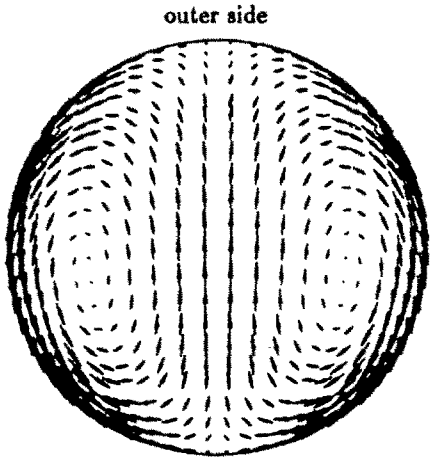

Fig. 1: Vapor flow structure in the cross-section: $R_c/R = 42$, $Re = 1.07 \times 10^6$, $\beta = 15^\circ$ [13]

The aim of the present study is to clarify the effects of a bend on the dispersed flow film boiling, particularly on its feature of wetting through the detailed measurement of system parameters. In the following, wetting characteristics are described firstly. The physical mechanism responsible for the appearance of wetting is then discussed through the analysis of the droplet dynamics. A parametric study is finally given to identify the governing factors for the wetting phenomenon in bends.

Experimental Apparatus and Procedure

The experiments were carried out in a refrigerant Freon-12 two- phase flow test facility illustrated in figure 2.

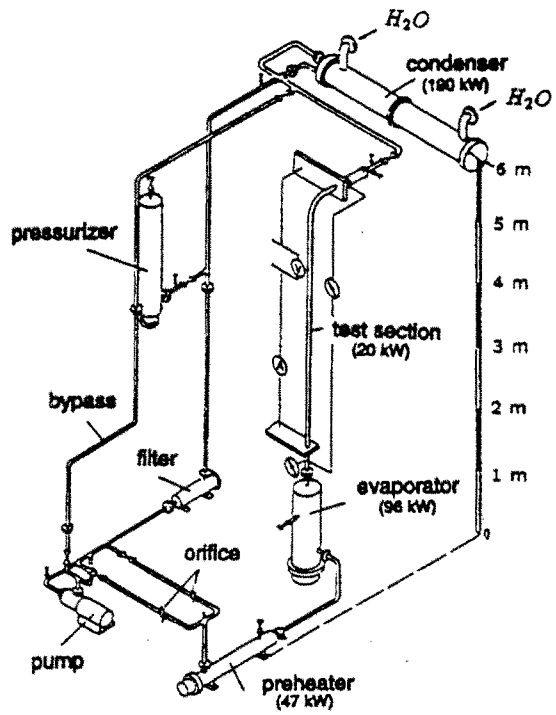

Fig. 2: Sketch of refrigerant Freon-12 test loop

Driven by a centrifugal pump, the refrigerant passes firstly through a control valve and an orifice flowmeter where the mass flux is adjusted and measured. It then enters a preheater in which the fluids is heated to a level of a few Kelvins below the saturation point. Two-phase flow is produced in a high-power evaporator, and a pattern of annular flow is arranged to appear at its outlet. The dispersed droplet flow is formed through the dryout of the annular flow in the test-section. It is further developed along the 2.5 m vertical part before it enters the bend where extensive measurements are performed. The two-phase mixture is finally condensed in a water-cooled condenser. Then the pure liquid passes through a filter and flows back to the pump inlet. The system pressure in the loop is controlled by a pressurizer.

Figure 3 shows the layout of the test-section and the instrumentation. The stainless steel test-section has an inner diameter of 28.5 mm and a wall thickness of 2.6 mm. It contains a 3.5 m long vertical part and a 90-deg bend. Two different bends were employed during the experiments, one with a radius of 0.4 m and another with 0.6 m. The ellipticity along the bend is less than 4% and the maximum deviation in wall

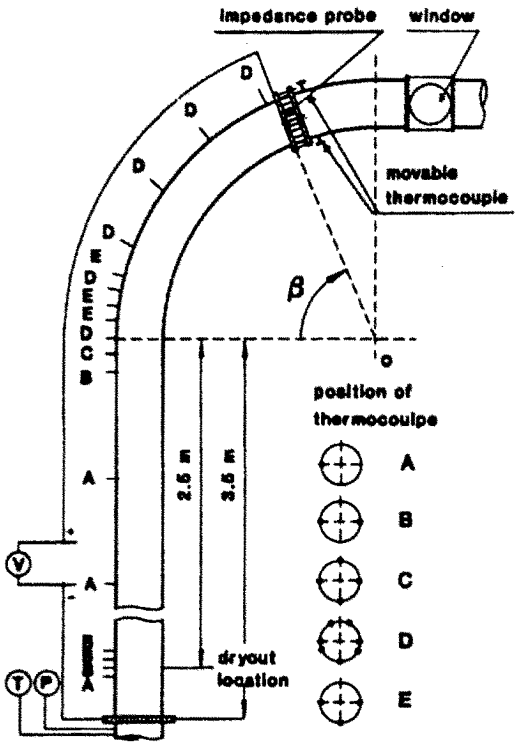

Fig. 3: Layout of the test-section

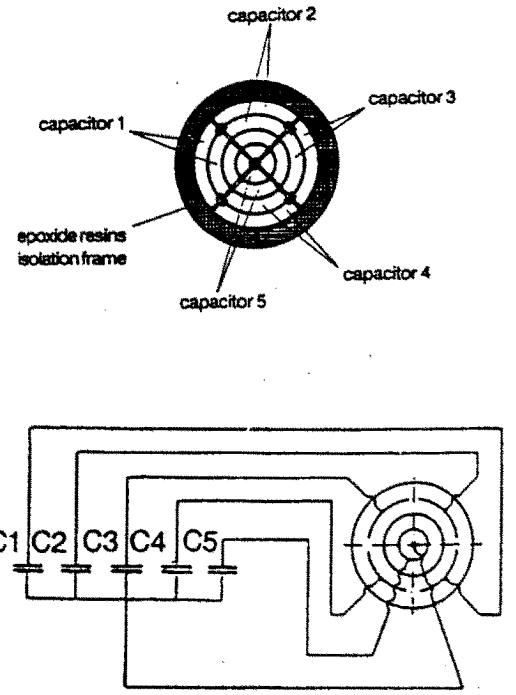

Fig. 4: Structure of the impedance probe

thickness is less than 4.6%. The whole test-section is Joule-heated by direct current.

The wall temperatures are measured by NiCr-Ni thermocouples of 0.5 mm diameter, spot welded on the outside surface of the tube at different axial and circumferential locations (see figure 3). Right after the impedence probe two movable bare thermocouples are installed for the probe calibration in single phase liquid and single phase vapor states.

A method of local liquid fraction measurement by an impedance probe is used to determine the liquid distribution in five different regions of the cross-section. Figure 4 shows the structure of the probe. It is composed of four thin concentric rings divided and wired together to constitute five separate capacitors in which a nearly homogenous electric field is established. Different capacitors are electrically isolated and supported by an epoxide frame. Supplied with 1 MHz high frequency voltage, these capacitors are gauged with a Boonton type 72BD digital capacitance meter with a precision of 0.15% of the full range. According to the theoretical analysis of Maxwell [11] for dispersed droplet flow, the liquid fraction 1-ε can be deduced from the two-phase dielectric constant e via capacitance measurement

$$1-\varepsilon=\frac{e-e_g e_l+2e_g}{e+2e_g e_l-e_g} \qquad (1)$$

where e_l, e_g denote the dielectric constants for pure liquid and pure gas. However, once the dispersed droplet flow forms a liquid film on one of the electrodes due to the droplet impingement, uncertainty may exist by using equation 1. Wang [12] gave a detailed error analysis for this measuring technique. Based on the assumption that the measured capacitance is the resultant from two capacitors in series, i.e. one formed by the pure liquid film, and another by the homogenous dispersed two-phase mxiture, he showed that the Maxwell correlation still gives a good indication of liquid fraction as long as the liquid film is thin. For example, the relative error accounts for about 9% even if the liquid film occupies 10% of the total liquid. It is therefore concluded that this measuring technique is appropriate for the present study.

The test conditions are summarized as follows:

mass flux G	400-2000 kg/m^{2}s
wall heat flux $\dot{q}_w$	20 - 60 kW/m^2
curvature ratios Rc/R	14, 28, 42
reduced pressure P/Pc	0.23

Experimental Results and Discussion

Wetting Characteristics

The wetting phenomenon in the 90-deg circular heated bend for a typical experimental run is illustrated in figure 5. Similar behavior is observed for othe r runs of dispersed flow under intermediate to large mass fluxes and small to intermediate wall heat fluxes.

Figure 5a shows the wall temperature distributions along the bend at three different positions of the circumference. For reference, the saturation temperature is also presented. Figure 5b gives the results of liquid distributions from the impedance probe for four different regions in the cross-section and four angular positions in the axial direction. As can be seen, a non-symmetric pattern of liquid distribution appears immediately after the bend entrance. The centrifugal forces bring a large amount of liquid droplets from the tube center to the outer side of the bend, resulting in an increased droplet concentration at that region. Because of the cooling effect by the droplet evaporation in the thermal boundary layer, the local heat transfer by film boiling is improved and consequently a clear wall temperature gradient in circumference is observed. However, the deposition rate of droplets at this stage is not high enough to induce any wet collision. The flow maintains the similar features as in a vertical film boiling channel, except for the skew structure of the droplet distribution (see A in figure 5c).

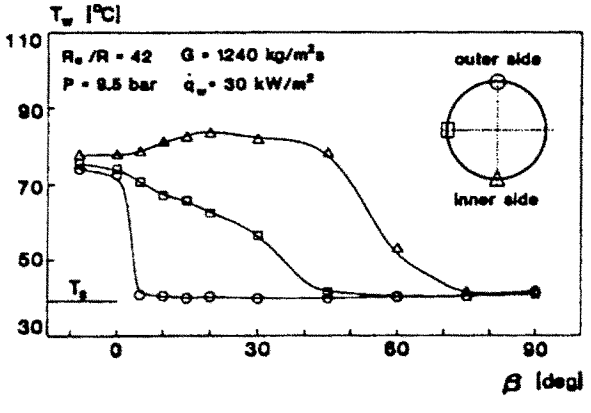

Fig. 5a: Wall temperature distribution

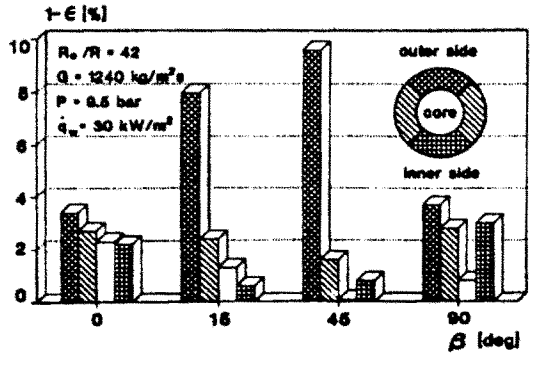

Fig. 5b: Liquid distribution

As the liquid deposition on the outer wall increases, the thermal boundary layer becomes thinner, and the temperature gradient in this layer becomes smaller. When liquid droplets are not subjected to high evaporation, and the thermal repelling forces due to the non-uniform evaporation [14] can no longer resist the centrifugal forces, droplets may impinge continuously on the outer wall leading to the onset of wetting. This process is demonstrated by the temperature distributions in which the outer wall is found to be suddenly quenched to a level near the saturation temperature. Further downstream, wetting is maintained by a sustained deposition of liquid droplets indicated by the liquid fraction measurement. During the development of the secondary flow of vapor phase, the interfacial shear stresses tend to stretch the liquid film along the circumference towards the inner side. This circulating motion of the liquid film is strengthened by the action of the gravitational force. Eventually, as indicated from the measurements, wetting is propagated from the outer to the inner side of the bend. The region where partial wetting and partial film boiling coexist is represented by B in figure 5c.

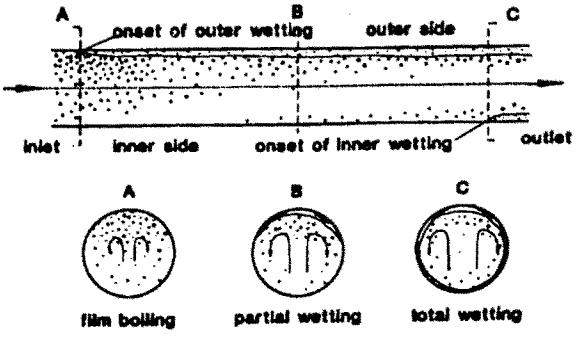

Fig. 5c: Wetting characteristics in the bend

Total wetting shown by C in figure 5c appears almost always in the later part of the bend. As revealed in figure 5b, most of the liquid is found to be close to the wall region. There are only a few droplets in the core of the tube. Different from the case in film boiling, heat transfer is significantly enhanced by the film evaporation.

Origin of Wetting - A mechanistic Study

The present measurements indicate that the dispersed flow entering the bend usually possesses a high vapor quality in excess of 0.8 and a low liquid fraction less than 0.1. The dispersed flow cooling dynamics are therefore closely connected with the behavior of individual droplets in the vapor stream and on the heated wall. Quantitative description of the droplet dynamics can be performed either by the Eulerian approach, in which droples are treated as a continuous phase and their motion is mathematically determined by the conservation equations for liquid and vapor, or by the Lagrangian approach, in which instantaneous movement of individual droplets is tracked by solving their equations of motion. The latter technique has been employed by the authors [12-13] and is used here to study the droplet behavior and its role contributing to the wetting phenomenon. For completeness of the present study, a brief description of this Lagrangian trajectory model is included at the end of the paper.

Figure 6 gives a tentative evaluation of droplet behavior in the heated bend. Wall temperature in this case is set to be higher than the Leidenfrost temperature. Two different groups of computations

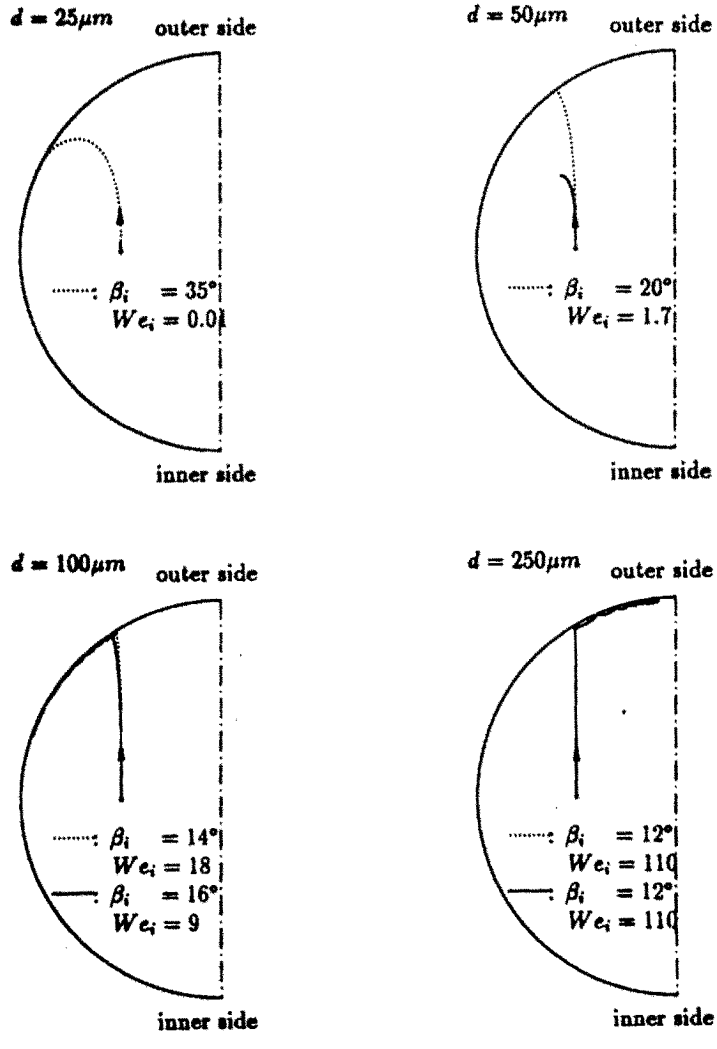

Fig. 6: Behaviour of droplet motion in the bend: $R_c / R = 42$, P = 9.5 bar, Reg = 1.07 x 106, = 60 kW/m^2, T $\dot{q}_w$ = 60 kW/m^2, $T_{g,o} - T_s$ = 30°C

were performed. The continuous lines represent the computations with evaporation effect, simulating the cases in high non-equilibrium flows. The dotted lines represent the computations without evaporation effect, corresponding to the cases in equilibrium flows. It should be noted that these two extreme conditions may apply to different regions in the bend. For example, the former holds true to the early stage of the bend, whereas the latter is valid in regions where extensive evaporation of liquid happens, e.g. in the outer region in most part of the bend. It should be mentioned that the results demosntrated here do not include the turbulence effect of vapor phase. However, it has been revealed by the authors elsewhere [13] that the droplet behavior can still be well predicted by considering the mean effect of the vapor phase over a large spectrum of droplets.

In the figure, droplet trajectories are presented for droplet dimensions from 25 μm to 250 μm. For all four cases without the evaporation effect, droplets are subjected mainly to the centrifugal forces in most part of the bend. The secondary flow effect, appears to be important for relatively small droplets in the limited region near the wall. For the cases with thermal effect, smaller droplets between 25 μm and 50μm tend to disappear by strong evaporation before reaching the outer wall. However, for slightly larger droplet of 100 μm, the evaporation process appears to have less influence in the core region. The droplet evaporates mainly in the wall region on its way towards the inner side by the secondary vapor flow. For even larger droplet of 250 μm, the centrifugal effect dominates the whole process of droplet motion. Because of the high impinging Weber number, a breakup of the droplet on the wall may occur. According to the present analysis, satellite droplets from the broken body remain further centrifugally governed and migrate towards the symmetric plane due to their high tangential momentum. In addition, it is noted that even in the present case of high wall temperature and temperature gradient near the wall, the thermal repelling force evaluated by the model does not have a comparable magnitude with the centrifugal force to reject the droplet from the wall. This seems to suggest that the total evaporation effect may be more important than the thermal repelling effect for preventing droplets from the wall.

Figure 7 shows the deposition velocities of different droplets on the outer wall of the bend. The inlet droplet sizes used are 100, 130, 200 μm, among which the second one is a representative droplet size under the same boundary condition as in the figure 5 [12]. Deposition velocity distribution is computed by releasing the droplets of the same size at different positions of the symmetric plan at the bend inlet. Their deposition angles and velocities are then recorded. For comparison, the deposition velocity of droplets in the vertical channel is also given in the same figure. It is calculated from the correlation

$$\frac{V_{d,i}}{V_g} = \frac{0.023}{Re_g^{0.1}} \tag{2}$$

which was developed from measurements [15] and extended to the analysis of film boiling [16].

It can been seen that for all droplets of different sizes, there is a region in the early part of the bend where rapid increase of droplet deposition velocity exists. In this limited region, the deposition velocity increases from the value in vertical film boiling to an order-of-magnitude higher one. Moreover, this region is found to coincide with the high quenching region in figure 5a. This reflects the importance of droplet direct impact on the wetting process in the bend.

To summarize the aforementioned mechanistic study together with the measurements described in the previous section, one can come to the conclusion that droplets in the bend exhibit high deposition velocity. The larger the droplets are, the easier it is for them to centrifugally impinge on the outer wall. Wetting is initiated by the direct impact of droplets and maintained by a sufficient deposition rate under which individual liquid disks are linked together to constitute a continuous liquid film.

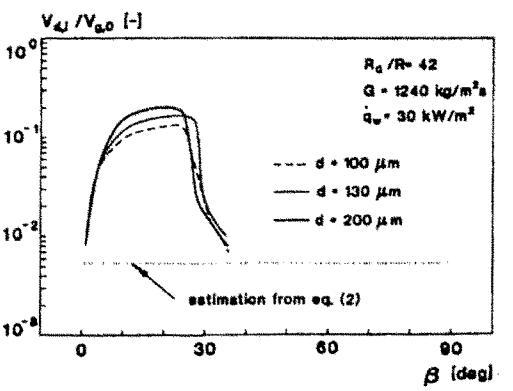

Fig. 7: Droplet deposition velocities in the bend

Parametric effects on the wetting phenomenon

As discussed in the last two sections, the evaluation of dispersed flow film boiling relies on the detailed information like droplet size, droplet concentration, slip ratio, bulk vapor flow structure, vapor superheating, etc. Therefore a quantitative establishment of a criterion for the onset of wetting is only possible after extensive measurements of these local parameters. This task seems to exceed the scope of the present paper. What we are to present here is a parametric study on the wetting phenomenon. Effects of the most important parameters: wall heat flux, mass flux and curvature ratio, which control the aforementioned local parameters, are discussed in the following in order to further clarify the governing factors for the onset of wetting and the wetting propagation.

Effect of heat flux

Figure 8 shows the outer wall temperature distributions at different wall heat fluxes. As can be seen, increasing the heat flux leads to a delay of wetting. Further increase of heat flux up to 50 kW/m^2 results in a totally dry wall along the 90-deg bend. This implies that for a given droplet deposition flux, there seems to be a critical temperature gradient in the boundary layer beyond which a continuous accumulation of liquid on the wall is prevented due to droplet evaportion and repelling effects. Under the present condition, droplets at the bend inlet have the magnitude of about 250 μm [12]. According to figure 6, a strong interaction of droplets with the heated wall is expected. As long as the heat flux remains small or moderate (See 20 to 40 kW/m^2 in the figure), the temperature gradient in the boundary region is small enough to allow droplets to penetrate the thermal barrier and form a stable film on the outer wall. On the contrary, at the high heat flux of 50 kW/m^2, droplets impinge on the wall and break into small pieces which easily evaporate in the high superheated wall region. Although there is some improvement in heat transfer, no wetting appears on the outer wall in this case.

The experimental results displayed here confirm the importance of the temperature gradient in the boundary layer to the wetting. A stable wetting appears always under small wall heat fluxes, i.e. small temperature gradients.

Effect of mass flux

Another imortant parameter affecting the onset of wetting is the mass flux. Figure 9 shows the outer wall temperature distributions for different mass fluxes. The onset of wetting is found respectively in the early part of the bend for mass fluxes from 2000 to 680 kg/m^{2}s, whereas no wetting is observed at G of 400 kg/m^{2}s. This may be attributed to the effects of droplet deposition flux and wall superheat. As known from dispersed flow film boiling, increasing the mass flux increases the flow Reynolds number and the liquid population whereas it decreases the wall superheat and the liquid droplet size. According to the previous analysis, the first three factors are favorable and the last one is negative to the wetting. Their total effect on the droplet deposition velocity is shown in figure 10 by the droplet trajectory model for the two mass fluxes of 680 kg/m^2 and 1240 kg/m^{2}s. It can be seen that the larger mass flux corresponds to a higher droplet deposition velocity due to

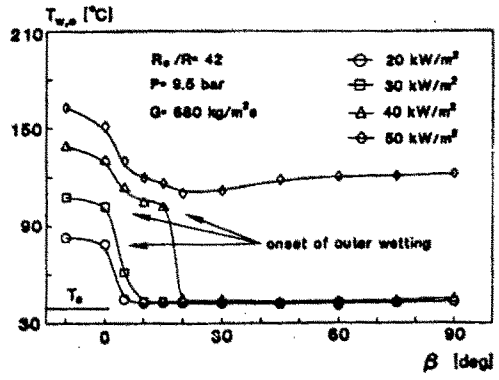

Fig. 8: Effect of heat flux on the wetting

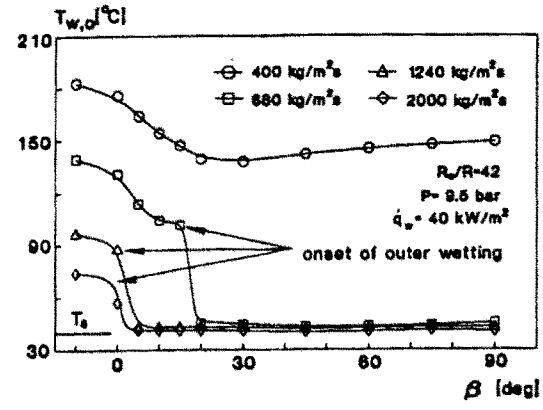

Fig. 9: Effect of mass flux on the wetting

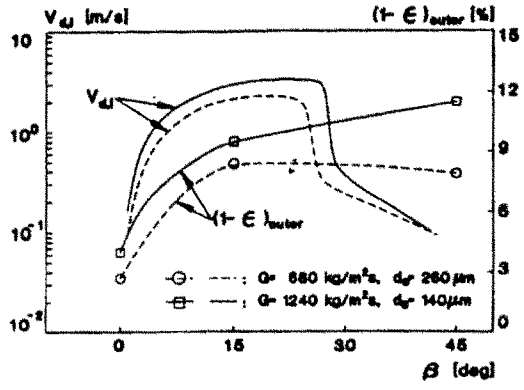

Fig. 10: Droplet deposition velocities and liquid fractions at different mass fluxes

stronger centrifugal acceleration. Besides, measurements of local liquid fraction shown in same figure indicate a higher liquid concentration at the outer region (see figure 5b for definition) for this mass flux. Consequently, the droplet deposition flux for the larger mass flux is much higher than that for the smaller mass flux. The bend wall with smaller superheating at larger mass fluxes is therefore much easier to be wetted. For the mass flux of 2000 kg/m^{2}s, wetting takes place immediately after the bend inlet.

Effect of curvature ratio

In addition to heat flux and mass flux, the curvature ratio, i.e. bend to tube radius ratio, is also important to the wetting phenomenon. Figure 11 presents the inner wall temperature distributions for three different bends. The region for the onset of wetting on the outer wall is found to appear within the first five degrees from the entrance without much differences in these bends. The issue to be discussed here is the speed of wetting in the circumference. It is noted from the figure that although the outer wetting positions are nearly the same, the wetting speeds in circumference in terms of the angular angle are quite different for the three bends. Wetting at the inner wall appears 15 degrees earlier for the curvature ratio of 42 than for the ratio of 28. Liquid film even does not reach to the inner wall within the 90-deg bend for the curvature of 14. Such behavior of the liquid film development can be explained by analyzing the circumferential velocities of the liquid film. Figure 12 illustrates the computational results on the ratio of the maximum secondary flow to the mean primary flow in different bends [12]. They were obtained in the same Reynolds number region as in figure 11. As the film velocity in circumference depends partially on the interfacial shear stress, or the secondary flow of the vapor phase, it can be postulated from figure 12 that large-radius bends have smaller film velocities. For example, the film velocity in the large radius bend (Rc/R = 42) may be about 20% smaller than that in the bend of Rc/R = 28. Including additional effects of the gravitational force, such difference in film velocity could be reduced in these two bends. It is apparent that the effect of a maximum 20%-decrease in film velocity can be covered up by the effect of a 50%-increase in bend radius when calculating the relative circumferential film velocity within a certain bend angle $\Delta\beta$ for these two bends. Therefore the propagation of liquid film in circumference appears to be faster in the large radius bend for the same bend angle.

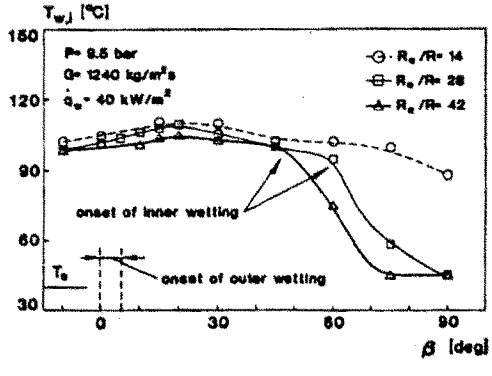

Fig. 11: Effect of curvature ratio on the wetting

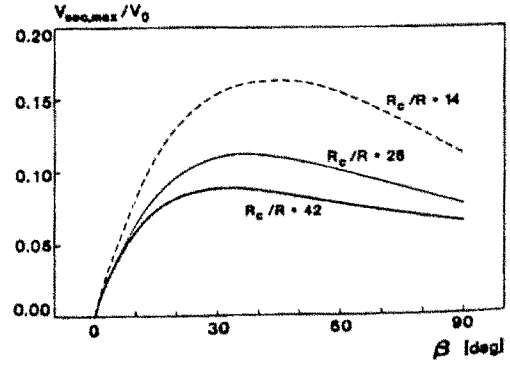

Fig. 12: Secondary flows of the vapor phase in different bends

Conclusions

Wetting is one of the most distinguished behaviors of dispersed flow in circular bends. This paper examines the physical mechanism of the wetting phenomenon by measurements of the wall temperature and the liquid concentration, and by the theoretical analysis of droplet dynamics. It is found that the initiation of wetting in a bend is attributed to the direct impingement of droplets on the heated wall. Droplet deposition flux and the temperature gradient in the thermal boundary layer are shown to be the two governing factors affecting the onset of wetting. Controlled by the secondary vapor flow and the gravitational force, wetting is propagated along the circumference from the outer side towards the inner side of the bend.

Nomenclature

A	=	surface area vector
B	=	Spalding number $B = \frac{h_g - h_{g,s}}{h_g}$
C_D	=	drag coefficient
d	=	droplet diameter
D	=	tube diameter
e	=	relative dielectric constant
e	=	unit vector
F	=	force vector
g	=	gravitational acceleration
G	=	mass flux
h	=	specific enthalpy
h_{fg}	=	latent heat
m_d	=	mass of droplet
P	=	pressure
P_c	=	critical essure
Pr	=	Prandtl number, $Pr = \frac{c_p \mu}{\lambda}$
$\dot{q}$	=	heat flux
$\dot{Q}$	=	heat convection rate
r	=	radial coordinate
R	=	tube radius
R_c	=	bend radius
Re	=	Reynolds number, $Re = \frac{\rho V D}{\mu}$
Re_d	=	droplet Reynolds number $Re_d = \frac{\rho_g \lvert V_g - V_d \rvert d}{\mu_g}$
t	=	time
T	=	temperature
V	=	velocity vector
$V_{d,i}$	=	droplet deposition velocity
V_r	=	relative velocity
We	=	Weber number $We = \frac{\rho_l V_d^2 d}{\sigma}$

Greek Symbols

α	=	heat transfer coefficient
β	=	bend angle
ε	=	void fraction
θ	=	polar coordinate
μ	=	dynamic viscosity
ρ	=	density

Subscripts

d	=	droplet
g	=	vapor
i	=	inner
l	=	liquid
o	=	outer
s	=	saturation
w	=	wall
O	=	mean parameter at bend inlet

References

1. Mayinger, F. Stromung und Warmeubertragung in Gas-Flussigkeits- Gemischen, Springer Verlag, Wien (1982).
2. Chen, J.C. A short view of dispersed flow heat transfer in post- dryout boiling, Nucl. Eng. Design, 95, 375-383 (1986).
3. Aihara, T. Augmentation of convective heat transfer by gas-liquid mist, Proc. 9th Int. Heat Transfer Conf., Jerusalem, 1, 445-461 (1990).
4. Baumeister, K.J. and Simon, F.F. Leidenfrost temperature - Its correlation for liquid metals, cryogens, hydrocarbons and water, J. Heat Transfer, 109, 43-48 (1973).
5. Bolle, L. and Moureau, J.C., Spray cooling of hot surface, in Multiphase science and technology, 1, 1-98 Edts: Hewitt, G.F., et al. Hemisphere, Washington (1982).
6. Hein, D. Modellvorstellungen Zum Wiederbenetzen durch Fluten, Dissertation, Universitat Hannover (1980).
7. Chan, A.M.C., and Banerjee, S., Refilling and rewetting of hot horizontal tube, J. Heat Transfer, 103, 281-292 (1981).
8. Plummer, D.N., Iloeje, O.C., Griffth, P. and Rohsenow, W.M. A study of post critical heat flux heat transfer in a forced convection system, GE Technical Report, No. 73645-80 (1973).
9. Groeneveld, D.C. and Stewart J.C. The minimum film boiling temperature for water during film boiling collapse, Proc. 7th Int. Heat Transfer Conf., Munchen, 4, 393-398 (1982).
10. Berger, S.A., Talbot, L. and Yao, L.S., Flow in curved pipes, Ann. Rev. Fluid Mech. 15, 461-512 (1983).

11. Hewitt, G.F., Measurement techniques in Handbook of multiphase systems, chapter 10, Edt: Hetsroni, G., Hemisphere, Washington (1992).
12. Wang, M.J., Phase distribution, secondary flow and heat transfer of dispersed flow in circular bends, Dissertation, Technische Univesitat Munchen, Verlag Shaker, Aachen (1993).
13. Wang, M.J. and Mayinger F., Post-dryout dispersed flow in curved channels - Bulk vapor flow, droplet dynamics and phase distribution, 28th European Two-Phase Flow Group Meeting, Paper C2, Hannover (1993).
14. Ganic, E.N. and Rohsenow, W.M., On the mechanism of liquid drop deposition in two-phase dispersed flow, J. of Heat Transfer, **101**, 288-294 (1979).
15. Liu, B.Y.H. and Ilori, T.A., Aerosol deposition in turbulent pipe flow, Environmental Sci. & Tech., **8**, 351-356 (1974).
16. Varone, A.F., and Rohsenow, W.M., Post dryout heat transfer prediction, Nucl. Eng. Design, **95**, 315-327 (1986).
17. Renksizbulut, M. and Yuen, M.C. Experimental study of droplet evaporation in a high-temperature air stream, J. Heat Transfer, **105**, 384-388 (1983).
18. Burns, A.D. and Wilkes, N.S., A finite difference method for the computation of flows in complex three-dimensional geometries, UKAEA Report No. AERE-R12342 (1987).

Appendix

A Theoretical Model of Droplet Motion

Droplet motion in the superheated vapor stream through the circular bend is analyzed by a Lagrangian simulation model coupling the force and energy balance of individual droplet. Because of the high-quality nature of the dispersed flow, the model employs the one-way coupling treatment, i.e. the presence of droplets does not modify the turbulent vapor fields. In addition, the model assumes that droplets remain spherical before and after impact on the wall. Forces due to virtual mass, Basset history integral, pressure gradient, Saffman and Magnus lifts as well as particle interactions are not taken into account. Thus the path of an evaporating droplet can be described by the following ordinary differential balance equations for energy:

$$h_{fg}\frac{dm_d}{dt} = -Q_{gd} \tag{A.1}$$

for force

$$\frac{d(m_d V_{d,i} e_i)}{dt} = F_i e_i \tag{A.2}$$

In equation (A.1), Q_{gd} is the rate of heat convection from superheated vapor to the droplet

$$\dot{Q}_{gd} = \pi d^2 \alpha_{gd} (T_g - T_s) \tag{A.3}$$

where the heat transfer coefficient α_{gd} is calculated using the correlation [17]

$$\alpha_{gd} = \frac{\lambda_{g,f}}{d}(2+0.57\,\mathrm{Re}_d^{0.5} Pr_{g,f}^{0.33})\,(1+B)^{-0.7} \tag{A.4}$$

In toroidal coordinate system (r,θ,β) shown in figure A.1, the derivative of the unit vector e with respect to time t for each coordinate is

$$\frac{de_r}{dt} = \frac{V_{d,\theta}}{r} e_\theta + \frac{V_{d,\beta}\cos\theta}{R_c + r\cos\theta} e_\beta \tag{A.5}$$

$$\frac{de_\theta}{dt} = -\frac{V_{d,\theta}}{r} e_r - \frac{V_{d,\beta}\sin\theta}{R_c + r\cos\theta} e_\theta \tag{A.6}$$

$$\frac{de_\beta}{dt} = -\frac{V_{d,\beta}\cos\theta}{R_c + r\cos\theta} e_r + \frac{V_{d,\beta}\sin\theta}{R_c + r\cos\theta} e_\theta \tag{A.7}$$

Introducing equations (A.5)-(A.7) into (A.2), and rearranging them lead to some extra terms. Among them, the combination of

$$m_d\left[\frac{V_{d,\beta}^2\cos\theta}{R_c + r\cos\theta}\right] e_r \quad \text{and} \quad m_d\left[\frac{V_{d,\beta}^2\sin\theta}{R_c + r\cos\theta}\right] e_\theta$$

which directs from the inner to the outer side of the curvature is much more significant than other terms, and is conventionally called the centrifugal force.

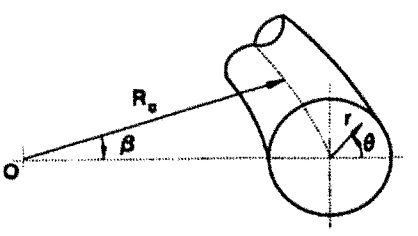

Fig. A.1: Coordinate system for the analysis of droplet motion

Other forces considered in the present model are the drag force

$$F_D = \frac{1}{4}\pi d^2 C_D \frac{1}{2}\rho_g |V_g - V_d| (V_g - V_d) \quad (A.8)$$

the buoyancy

$$F_b = \frac{1}{6}\pi d^3 (\rho_l - \rho_g) g \quad (A.9)$$

and the thermal repelling force due to non-uniform evaporation on the droplet surface [14]

$$F_{t,r} = \iint_A V_r (\rho_g V dA)$$

$$= \frac{\pi d^2 \alpha_{gd}^2}{4 h_{fg}^2 \rho_g} [(T_{g,2} - T_s)^2 - (T_{g,1} - T_s)^2] \quad (A.10)$$

In equation (A.8) the drag coefficient C_D is related to the droplet Reynolds number Re_d and the Spalding number B [17]

$$C_D = \frac{24}{Re_d} (1 + 0.2 Re_d^{0.63}) (1+B)^{-0.2} \quad (A.11)$$

where the factor $(1+B)^{-0.2}$ accounts for the reduction in drag due to the blowing effect of uniform evaporation. In equation (A.10), $T_{g,1}$ and $T_{g,2}$ are the vapor temperatures at the positions corresponding to the center of the front and the rear part of the droplet in the direction to the wall.

Equations (A.1) and (A.2) for energy and force balance together with the equations for Lagrangian velocity components.

$$\frac{dr}{dt} = V_{d,r} \quad (A.12)$$

$$\frac{d\theta}{dt} = \frac{V_{d,\theta}}{r} \quad (A.13)$$

$$\frac{d\beta}{dt} = \frac{V_{d,\beta}}{R_c + r\cos\theta} \quad (A.14)$$

constitute an equation matrix, which was solved by the 4th-order Runge-Kutta algorithm to obtain the droplet trajectory in the bend.

The single-phase turbulent vapor fields used in the analysis were obtained preliminary by solving the conservation equations for mass, momentum and energy equation with appropriate boundary conditions and the standard k-ϵ turbulence model. The computations were carried out using the finite-difference code FLOW3D [18]. Numerical details are given in ref. 12.

Interaction of the droplet with the hot wall are simulated following a graphical correlation for the rebounding velocity [5]. A breakup criterion based on previous experimental data is also included in the model. It is assumed that the breakup number of impinging droplet is 1 for $We_i < 2$ for $30 \leq We_i \leq 80$ and 10 for $We_i > 80$. Satellite droplets are still treated as spherical practices.